Fuel Processing Technology 156 (2017) 253–264

Contents lists available at ScienceDirect

Fuel Processing Technology

journal homepage: www.elsevier.com/locate/fuproc

Research article

Adsorption and activation of CO and H_2, the corresponding equilibrium phase diagrams under different temperature and partial pressures over Cu(100) surface: Insights into the effects of coverage and solvent effect

Riguang Zhang, Xiaobin Hao, Tian Duan, Baojun Wang *

Key Laboratory of Coal Science and Technology of Ministry of Education and Shanxi Province, Taiyuan University of Technology, Taiyuan 030024, Shanxi, PR China

ARTICLE INFO

Article history:
Received 22 April 2016
Received in revised form 9 September 2016
Accepted 10 September 2016
Available online 21 September 2016

Keywords:
Cu(100) surface
CO
H_2
Adsorption
Surface coverage
Solvent effect

ABSTRACT

The adsorption and activation of CO and H_2 at different coverage over Cu(100) surface under the vacuum and liquid paraffin conditions have been investigated using DFT calculations together with ab initio thermodynamics. It is found that the stepwise adsorption energies of CO decrease with the increasing of coverage, and CO prefers to desorption rather than its dissociation in vacuum and liquid paraffin, which are independent on the reaction environment. H_2 in vacuum is the dissociative adsorption at the coverage less than or equal to 3/12 ML, but until to the coverage of 6/12 ML in liquid paraffin, indicating that solvent effect can make more H_2 molecules become the dissociative adsorption; moreover, solvent effect is in favor of stabilizing the adsorption configurations of dissociated H atoms. Further, the equilibrium phase diagrams illustrate the relationship between the stable CO(H_2) adsorption with the temperatures and CO(H_2) partial pressure on Cu(100) surface in vacuum and liquid paraffin. It is concluded that H_2 exists in the form of H atoms, and CO is the molecular adsorption, which provide the reasonable explanations for many studies related to CO and H_2 on Cu catalyst under the realistic condition.

1. Introduction

Due to the extensive sources of syngas and its low cost, the production of alternative fuels from syngas (CO + H_2) conversion has been considered as a promising synthetic process [1–3], in which syngas can be converted to diverse chemical products, such as dimethyl ether [4–6], methanol [7,8], ethanol [9,10] and F-T synthesis products [11,12], and so on. Considering the high cost of precious metals, Cu-based catalysts, as economically viable of industrial catalysts, have been widely used because of their high activity for vapor-phase hydrogenation reactions [13,14], as well as the high activity and selectivity toward methanol [15,16]; moreover, Cu/ZnO/Al_2O_3 and CuO/ZnO/Al_2O_3 catalysts have been widely used, which present the promising results for methanol, ethanol and DME formation from syngas [16–18].

There are two reactors to synthesize methanol [7,16], DME [18–20], ethanol [9,21], etc. from syngas, one is fixed bed reactor with gas phase method, and the other is slurry reactor with liquid phase method, which can efficiently remove heat, keep the isothermal condition, and improve the energy utility in the highly exothermic reactions; meanwhile, the catalyst in the slurry reactor needs to be dispersed in liquid medium, such as the inert liquid paraffin. However, the effect of liquid environment on the adsorption and activation of CO and H_2 is still unclear; in this study, the liquid paraffin is considered to mimic the effect of solvent environment in the slurry reactor.

For syngas conversion, the adsorption and activation of CO and H_2 are not only the initial step, but also the key steps. The interactions of CO and H_2 molecules with Cu(111), (110) and (100) surfaces in vacuum and liquid paraffin have been examined by experimental and theoretical researchers [19,22–30], however, these studies mainly focus on the low coverage. On the other hand, it is well known that the temperature and gas partial pressures have dramatic influence on CO/H_2 adsorption and dissociation on metal surfaces. Lately, Jiao et al. [31–36] applied ab initio thermodynamics method to consider the effects of temperature and pressure on CO and H_2 adsorption and dissociation at different coverage on Fe, Mo and Ru-based catalysts; and further plotted the phase diagrams of stable CO and H_2 adsorption with the coverage on these surfaces, these results provide the useful thermodynamic information for CO and H_2 adsorption states at high temperature and pressure, which is of importance for industrial applications.

Up to now, to the best of our knowledge, a detailed understanding about the effect of coverage on the adsorption and activation of CO and H_2 over Cu catalyst, as well as the effect of temperature and CO/H_2 partial pressure on CO/H_2 surface coverage is still lacking under the vacuum and liquid paraffin conditions, respectively. Thus, we need to understand the following new insights into CO and H_2 adsorption and dissociation on Cu(100) surface: (1) When the coverage of CO and H_2

* Corresponding author at: Taiyuan University of Technology, No. 79 Yingze West Street, Taiyuan 030024, PR China.
E-mail addresses: wangbaojun@tyut.edu.cn, quantumtyut@126.com (B. Wang).

http://dx.doi.org/10.1016/j.fuproc.2016.09.005
0378-3820/

changes from the low coverage to the high coverage, whether the adsorption site, adsorption geometry and adsorption energy begin to change or not; (2) Since CO dissociation for syngas conversion on Cu surface at low coverage has not been achieved, whether CO dissociation at high coverage on Cu surface occur or not, in which the high CO coverage means the high CO pressure under the realistic condition. (3) Since the characterization of CO and H_2 adsorption at very low coverage (0.083 ML, 0.167 ML) is very complex in experiment, DFT calculations become an optimal method for the studies about CO and H_2 adsorption at different coverage on Cu surface. (4) What are the most stable adsorption configurations of CO and H_2 on Cu(100) surface at different coverage, whether the existence forms of CO and H_2 have changed or not? (5) How does the solvent affect CO and H_2 adsorption at different coverage on Cu surface? (6) How does the temperature and CO/H_2 partial pressure affect the surface CO/H_2 coverage on Cu surface?

For Cu catalyst, under the reducing conditions, the transmission electron microscopy (TEM) have shown that Cu particles expose primarily Cu(111) and Cu(100) surfaces [37,38]; moreover, Cu(100) surface may be more active, for example, the catalytic activity for H_2O and CO_2 follow the order of Cu(100) > Cu(111) in the water-gas shift (WGS) reaction, which may be attributed to the more open surface and more coordinative unsaturated sites of Cu(100) surface [13,22]. Thus, Cu(100) surface is chosen to model Cu catalyst in this study; meanwhile, in order to probe into the effects of coverage and solvent effect, as well as the effect of temperature and CO/H_2 partial pressure on CO/H_2 surface coverage, density functional theory (DFT) calculations together with atomistic thermodynamics have been employed to systematically investigate the adsorption and activation of CO and H_2 at different coverage over Cu(100) surface under the vacuum and liquid paraffin conditions, as well as the corresponding equilibrium phase diagrams under different temperatures and CO/H_2 partial pressures.

2. Computational details

2.1. Surface model

Cu(100) surface is cleaved from the experimental crystal structure with the lattice parameter of 3.620 Å [37], which may introduce unnecessary strain on the surface, and leads to the error in adsorption energies and other parameters compared to Cu(100) surface cleaved from the optimized primitive cell, as listed in Table S1, our results show that the strain of the surface has the negligible difference for the adsorption energies and surf.-Carbon distances of CO adsorption at different coverage compared to that on Cu(100) model cleaved from the optimized lattice constant of 3.615 Å (details in the Part 1 of Supplementary material). On the other hand, the effects of vacuum layer, slab thickness and surface size on CO adsorption energy have been tested in vacuum, as listed in Table S2, where CO is adsorbed at the favorable bridge site.

On the basis of test results, taking calculation efficiency and the reliability into consideration, a periodic $p(3 \times 4)$ supercell that containing four-layers Cu atoms has been employed. In our calculations, the bottom two layers of Cu(100) surface are fixed in their bulk positions, and the top two layers together with adsorbed species are relaxed. In order to avoid the interactions, 12 Å vacuum layer is inserted between the periodically repeated slabs. Three different adsorption sites on Cu(100) surface are presented in Fig. 1: Top, Bridge and 4-Fold hollow.

2.2. Calculations methods

All DFT calculations have been performed using $Dmol^3$ program package in Materials Studio 4.4 [39,40], since it is generally agreed that DFT methods give relatively accurate results for solid-state systems [41]. The calculations are carried out with the generalized gradient approximation with Perdew-Wang exchange–correlation functional (GGA-PW91) [42,43]. As listed in Table S3, the results for CO adsorption with different coverage at the different sites on Cu(100) surface obtained by PW91 functional qualitatively agree with the experimental studies by Pritchard [44] using low energy electron diffraction, which observed the bridge-bonded CO at low coverage on Cu(100) surface. Moreover, considering that PW91 functional overestimates CO adsorption energy on metal surface, CO adsorption at different coverage on Cu(100) surface using RPBE functional show that RPBE functional reduces CO adsorption energy, however, the predicted favorable top site is inconsistent with the experimental result [44]. Meanwhile, it is well known that RPBE functional worsens the descriptions of bulk crystals and surfaces [45–47], and gave a higher CO dissociation barrier than PW91 functional [35]. Therefore, PW91 functional is feasible to be applied to qualitatively investigate the adsorption and activation of CO and H_2 on Cu(100) surface in this study. C, O and H atoms are treated with an all-electron basis set, and the inner electrons of metal atoms are kept frozen and replaced by an effective core potential (ECP) [48,49]. The double-numeric polarized (DNP) basis set is employed [50]. Brillouin-zone integrations have been performed using $3 \times 2 \times 1$ Monkhorst-Pack grid and a Methfessel-Paxton smearing of 0.005 Ha. In addition, since our previous studies [51–53] have shown that DFT + D and DFT give the negligible differences for the adsorptions of CO and H_2 on Ni, Co and Rh surfaces at different coverage, namely, the vdw dispersion correction do not alter the results and conclusions, therefore, the vdw dispersion correction have not been considered for all energetics mentioned in this study.

The conductor-like screening model (COSMO) implemented into the $Dmol^3$ has been used to simulate the solvent effect [50,54]. In this model, the solute is put in the continuous medium where the dielectric

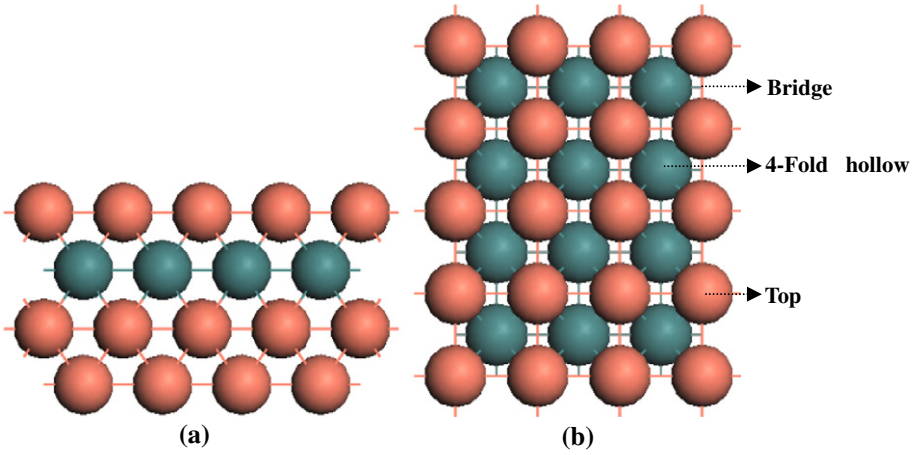

Fig. 1. The surface morphology and possible adsorption sites of Cu(100) surface. (a) Side view, (b) Top view.

constant is ε, and the liquid paraffin environment is replaced with the permittivity $\varepsilon = 2.06$. Complete LST/QST approach has been chosen to search for transition states of the reactions in order to determine the accurate barriers of the reactions [55]. In addition, transition state is confirmed by only one imaginary frequency.

The ab initio atomistic thermodynamics method can solve problems referring to real reaction conditions, which is proposed by Reuter and Scheffler [56,57]. Cu catalysts, as everyone knows, have been applied widely in methanol synthesis from syngas due to its good activity and high selectivity [58]. Methanol synthesis is usually carried out at the temperature of around 550 K [58–60]. Therefore, the temperature of 500 and 550 K for the thermodynamic calculations has been considered. The detailed descriptions about the calculations for the Gibbs free energy change of Cu surfaces after CO/H_2 adsorption under different temperatures and CO/H_2 partial pressure have been presented in the Part 2 of Supplementary Material.

The adsorption energy is defined as $E_{ads} = E_{slab} + E_{adsorbate} - E_{adsorbate/slab}$, where the $E_{adsorbate/slab}$ is the total energy of Cu(100) surface with the adsorbate; E_{slab} is the energy of the bare Cu(100) surface; and $E_{adsorbate}$ is the energy of adsorbate in gas phase. This definition indicates that the adsorption energy is more positive, the adsorption configuration is more stable. The desorption energies are equal to the negative values of the corresponding adsorption energies.

3. Results and discussion

3.1. CO and H_2 adsorption in vacuum

3.1.1. Adsorption of the single CO, C and O

Fig. S1 presents the most stable adsorption configurations of the single CO molecule, C and O atoms on Cu(100) surface, it is found that CO prefers to adsorb at the bridge site via C atom with the adsorption energy is 102.4 $kJ\cdot mol^{-1}$, which is very close to that at the top site (99.8 $kJ\cdot mol^{-1}$) and the 4-fold hollow site (99.7 $kJ\cdot mol^{-1}$). Our results are similar to Hussain's results that the adsorption energies of CO at the top (88.8 $kJ\cdot mol^{-1}$) and hollow (85.9 $kJ\cdot mol^{-1}$) sites are slightly lower than that (93.6 $kJ\cdot mol^{-1}$) at the bridge site, thus, CO can diffuse over different adsorption sites easily on Cu(100) surface due to the narrow gap of the adsorption energy [61]. Meanwhile, the C—O bonds of CO at the top, bridge, 4-fold hollow sites are perpendicular to the surface with its length elongated to 1.155, 1.171 and 1.195 Å from 1.141 Å in gas phase, respectively, as shown in Fig. S1(a), which agrees well with the previous studies [27].

C and O atoms are preferentially adsorbed at the 4-fold hollow site, as shown in Fig. S1(b) and S1(c); the average lengths of C—Cu and O—Cu bonds are 1.904 and 2.014 Å, respectively. However, when C or O atoms are placed at the bridge and top sites, the optimized structures are all converted into that at the 4-fold hollow site; In addition, previous studies have also shown that atomic O prefers to adsorb at the highly coordinated hollow site of Cu(100) surface [62].

3.1.2. Adsorption of CO at different coverage

In order to probe into CO adsorption at different coverage over Cu(100) surface in vacuum, it is necessary to obtain the most stable adsorption configurations at individual coverage. When CO molecules are adsorbed one by one over Cu(100) surface, the stepwise adsorption energy is defined as $\Delta E_{ads} = E_{COn/slab} + E_{CO} - E_{COn+1/slab}$, in which the temperature and pressure effects have been included. A negative ΔE_{ads} with n + 1 CO molecules adsorbed on the surface indicates the saturated adsorption with n CO molecules [63].

For the adsorption process of CO molecule, since the adsorption energy at the bridge site is close to that at the top site (99.8 $kJ\cdot mol^{-1}$), in order to find the most stable adsorption configurations at different coverage, the adsorption possibilities at the bridge and top site over Cu(100) surface at different coverage have been examined, as presented in Fig. S2. The most stable adsorption configurations of CO at different coverage and the stepwise adsorption energies in vacuum are presented in Fig. 2.

For $n_{CO} = 1$–4, the stepwise adsorption energies (102.4, 101.7, 100.2 and 100.4 $kJ\cdot mol^{-1}$) are very close, and all the adsorbed CO molecules are vertically located at their most stable bridge sites with the C—O bond perpendicularly to the surface, indicating that there are little lateral repulsive interactions between the adsorbed CO molecules. Thus, a high CO coverage is possible at the initial adsorption stage.

For $n_{CO} = 5$ and 6, ΔE_{ads} (92.0 and 87.1 $kJ\cdot mol^{-1}$) are smaller than those of the first four CO molecules. In the most stable configurations, although all CO molecules are still adsorbed at the bridge site, CO molecules begin to incline slightly, which may be attributed to the lateral repulsive interactions. The changes of ΔE_{ads} suggest that the lateral repulsive interactions between the adsorbed CO molecules gradually begin to affect CO adsorption when the coverage is greater than or equal to 5/12 ML.

For $n_{CO} = 7$, compared to $n_{CO} = 6$, all CO molecules are located at the top site in the most stable configuration with the stepwise adsorption energy of 72.5 $kJ\cdot mol^{-1}$ at the coverage of $n_{CO} = 7$, which indicates the most stable adsorption site changes from the bridge to the top.

For $n_{CO} = 8$, the stepwise adsorption energy (73.3 $kJ\cdot mol^{-1}$) is nearly equal to that (72.5 $kJ\cdot mol^{-1}$) at $n_{CO} = 7$; in the most stable configuration five CO molecules are adsorbed at the top site and three CO molecules are adsorbed at the bridge site, which indicates the top site become the main adsorption site at high coverage.

For $n_{CO} = 9$, the negative ΔE_{ads} (-24.3 $kJ\cdot mol^{-1}$) could be found, which means that when 8 CO molecules are adsorbed on Cu(100) surface, it reaches the saturated adsorption.

In general, with the increasing of CO coverage, the stepwise adsorption energies of CO decrease, namely, the corresponding desorption energies also decrease gradually. Hence, CO desorption becomes easier over Cu(100) surface with the increasing of CO coverage.

3.1.3. Dissociation and desorption of CO at different coverage

According to the stable adsorption configurations of CO molecules at different coverage over Cu(100) surface, the dissociation and desorption of these adsorbed CO molecules have been discussed to understand CO activation process. The stepwise adsorption energies equal to the reversed stepwise desorption energies, moreover, the desorption energies of the left CO molecules are calculated on the basis of the presence of others CO being dissociated for two or more CO molecules; Further, the comparison between the dissociation barrier and desorption energy of these absorbed CO molecules over Cu(100) surface have been considered.

For CO direct dissociation on Cu(100) surface, the reaction energy (ΔE) and activation barrier (E_a) have been calculated on the basis of the formulas $\Delta E = E_{FS} - E_{IS}$ and $E_a = E_{TS} - E_{IS}$; Here E_{IS} is the total energy of Cu(100) surface together with CO molecules, E_{FS} is the total energy of Cu(100) surface together with the co-adsorbed C and O atoms, and $E_{TS/Cu(100)}$ is the total energy of transition states for the direct dissociation reaction.

On the basis of the most stable adsorption configurations in Fig. 2, the dissociation barriers of all adsorbed CO molecules at the coverage from 1/12 to 3/12 ML have been calculated, and the corresponding structures are shown in Fig. 3; for the adsorption of CO at different coverage over Cu(100) surface in vacuum phase, the dissociation barrier, reaction energy and desorption energy obtained from DFT calculations are listed in Table 1, and the dissociation free energy, reaction free barrier and desorption free energy, as well as the dissociation and desorption rate constants at 500 and 550 K are listed in Table 2. In addition, the potential energy profiles for the dissociation of CO, 2CO and 3CO molecules on Cu(100) surface in vacuum is shown in Fig. S10.

For the single CO molecule dissociation, the adsorbed CO dissociates into C and O atoms via the transition state TS1-1, and C and O atoms are located at two adjacent 4-fold hollow sites in TS1-1; this elementary reaction is highly endothermic by 183.9 $kJ\cdot mol^{-1}$ with the dissociation

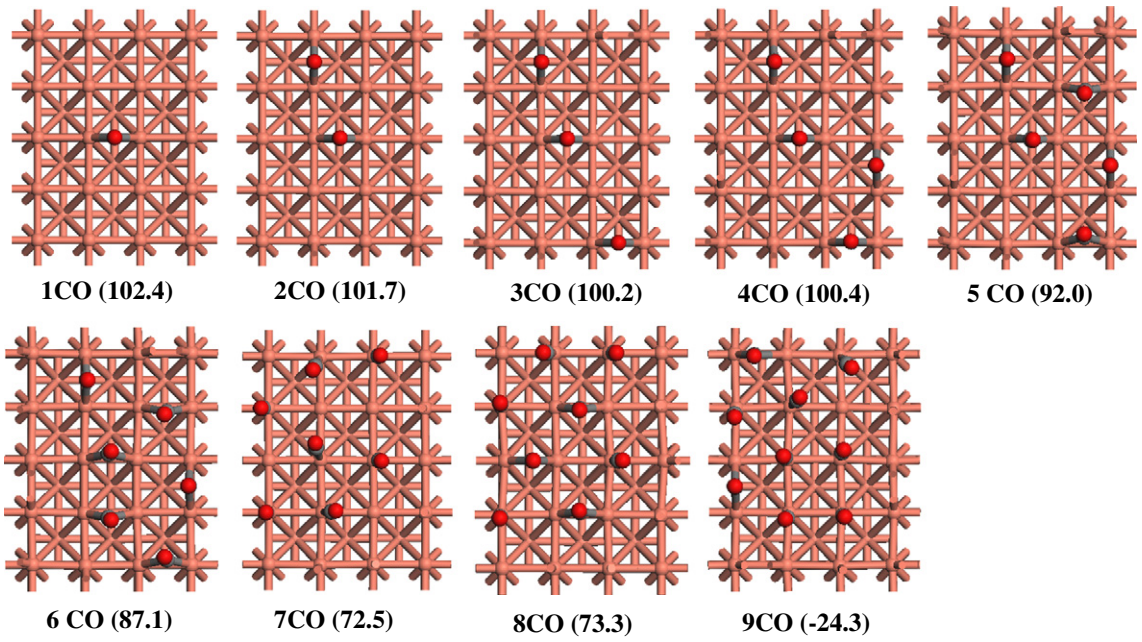

Fig. 2. The most stable adsorption configurations and energies of the stepwise CO adsorption on Cu(100) surface in vacuum (unit: kJ·mol^{-1}); Cu, C and O atoms are shown in the orange, grey and red balls, respectively.

barrier of 329.2 kJ·mol^{-1}, which is much higher than its desorption energy of 102.4 kJ·mol^{-1}, suggesting that CO dissociation is obviously unfavorable than its desorption at the coverage of 1/12 ML. Previous studies [64–66] have also shown that CO is very difficult to dissociate on Cu catalyst, for example, Sun. et al. [65] found that CO dissociation barrier on Cu(111) surface is 365.7 kJ·mol^{-1}. Therefore, the single CO

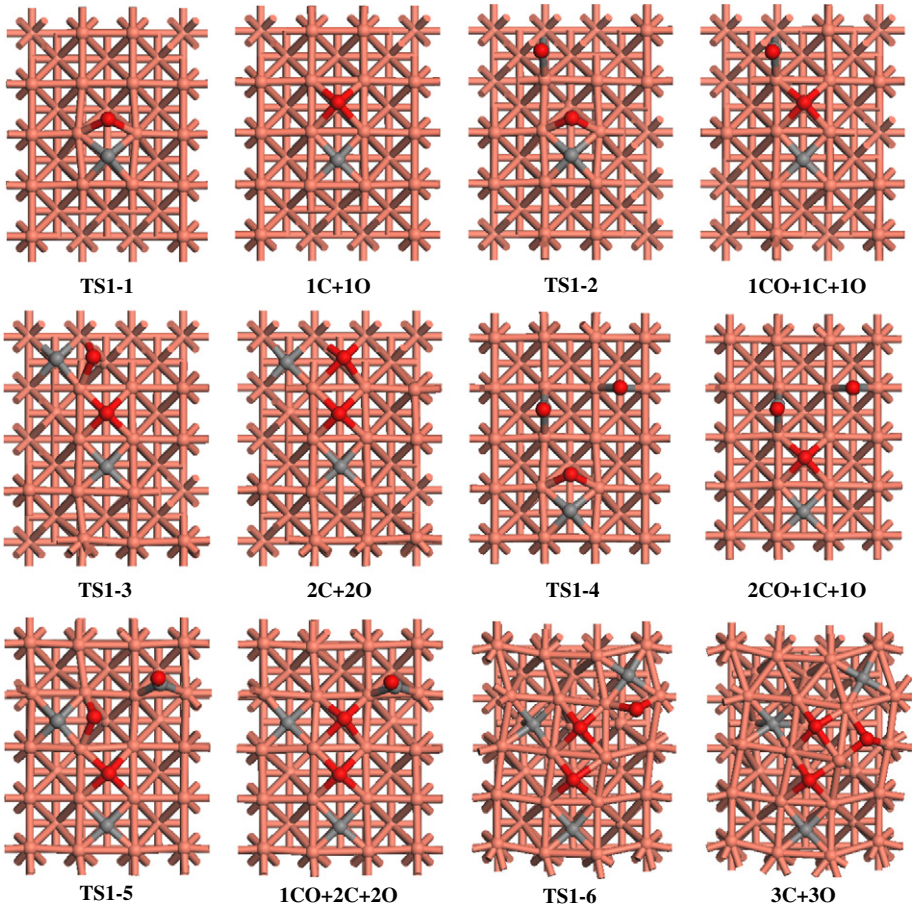

Fig. 3. Structures of transition states (TSs) and products involved in the dissociations of 1–3 CO molecules on Cu(100) surface in vacuum.

Table 1
Reaction energy (ΔE/kJ·mol^{-1}), dissociation barrier (E_a/kJ·mol^{-1}), desorption energy (E_{des}/kJ·mol^{-1}), the C—O bond length (d_{C-O}/Å), and the imaginary frequencies (v/cm^{-1}) corresponding to transition state for CO dissociation at different coverage over Cu(100) surface in vacuum phase and liquid paraffin.

	nCO	Dissociation route	d_{C-O}	ΔE	E_a	E_{des}	v
Vacuum	1CO	1CO → 1C + 1O	1.888	183.9	329.2	102.4	479.9i
	2CO	2CO → 1CO + 1C + 1O	1.936	195.9	319.0	101.7	434.3i
		1CO + 1C + 1O → 2C + 2O	2.006	200.7	346.6	99.8	410.0i
	3CO	3CO → 2CO + 1C + 1O	1.921	200.0	317.2	100.2	440.9i
		2CO + 1C + 1O → 1CO + 2C + 2O	1.963	225.9	364.8	96.1	430.3i
		1CO + 2C + 2O → 3C + 3O	2.063	203.8	373.0	70.8	352.7i
Liquid paraffin	1CO	1CO → 1C + 1O	1.903	180.9	328.2	150.0	498.0i
	2CO	2CO → 1CO + 1C + 1O	1.842	198.0	344.7	115.4	513.5i
		1CO + 1C + 1O → 2C + 2O	1.912	192.4	318.4	98.8	479.7i
	3CO	3CO → 2CO + 1C + 1O	1.852	199.5	349.6	82.6	508.0i
		2CO + 1C + 1O → 1CO + 2C + 2O	1.869	189.1	340.6	72.6	422.6i
		1CO + 2C + 2O → 3C + 3O	1.943	224.3	323.7	48.9	445.2i

desorption over Cu surface in vacuum is more favorable than its dissociation.

For two CO molecules dissociation, one of the adsorbed two CO molecules firstly dissociates into CO + C + O via TS1-2, in TS1-2, C and O are adsorbed at two adjacent 4-fold hollow sites; subsequently, the second CO molecule continues to dissociate via TS1-3 to the final state 2C + 2O, where two C atoms and two O atoms are all located at the 4-fold hollow sites. The corresponding dissociation barriers of these two CO molecules are 319.0 and 346.6 kJ·mol^{-1}, respectively, which are much higher than the corresponding desorption energies of 101.7 and 99.8 kJ·mol^{-1}, respectively. On the other hand, the dissociation of these two CO molecules is endothermic by 195.9 and 200.7 kJ·mol^{-1}, respectively. These results show that CO dissociation at 2/12 ML is also unfavorable than its desorption.

For the dissociation of three co-adsorbed CO molecules, these CO molecules stepwise dissociate into three C and three O atoms via the transition states TS1-4 ~1–6, the dissociation barriers are 317.2, 364.8 and 373.0 kJ·mol^{-1}, respectively, and these reactions are endothermic by 200.0, 225.9 and 203.8 kJ·mol^{-1}, respectively. The corresponding stepwise desorption energies are 100.2, 96.1 and 70.8 kJ·mol^{-1}, which are all obviously lower than their dissociation barriers, indicating that CO dissociation is still difficult at the coverage of 3/12 ML compared to their corresponding desorption.

On the basis of above results, we can obtain that with the increasing of CO coverage in vacuum, the dissociation barriers for the first CO molecule at different coverage have little change, however, the second CO dissociation barrier increased with the increasing of the coverage due to the presence of C and O on the surface; moreover, at a given coverage, the desorption energies of CO molecules gradually decrease with the increasing of C and O coverage. Further, the dissociation free barriers are also larger than the desorption free energy at different coverage at the temperature of 500 and 550 K, which also suggest that CO dissociation is unfavorable than its desorption. Moreover, the desorption rate of CO is far faster than its dissociation ones, the dissociation rate constants of the second CO dissociation decrease with the increasing of the coverage; Meanwhile, with the increasing of the temperature, the desorption and dissociation rate constant increases, while the changes of the desorption rate constant become small. Therefore, it is expected that CO dissociation will be unfavorable with the increasing of coverage, we can identify that CO dissociation is always difficult compared to its desorption on Cu(100) surface.

On the other hand, experimental studies have shown that CO dissociation over Cu surface in vacuum is less favorable than the desorption, namely, molecular adsorption CO dominantly exists on Cu catalyst. For example, Niemi et al. [67] have applied STM to study CO adsorption on Cu catalyst, suggesting that CO monomer and dimers always adsorbed over Cu(111) surface rather than its dissociation, which also be observed on the stepped vicinal Cu(211) system [68]. Kato et al. [69] have observed the tilted CO molecules to keep them away from each other using high-resolution electron energy-loss spectroscopy. These experimental results agree well with our calculated results about CO adsorption over Cu(100) surface at high coverage.

3.1.4. Adsorption of the single H_2 and H species

On the basis of the symmetry of H_2 molecule, parallel and vertical adsorption modes have been considered at the top, bridge and 4-fold hollow sites, respectively, as shown in Fig. S3. H_2 adsorption with the parallel mode at the 4-fold hollow site is the dissociative adsorption with the dissociated H atoms adsorbed at the bridge sites, as shown in Fig. S3(a); for H_2 adsorption with the parallel mode at the top and bridge site has only very weak adsorption energies of 6.5 and 11.2 kJ·mol^{-1}. Moreover, for H_2 adsorption with the vertical mode, H_2 molecule is far away from the surface with the adsorption energies about 13 kJ·mol^{-1}, and the H—H bond length equals to 0.755 Å compared to 0.747 Å in gas phase, as shown in Fig. S3(b).

Table 2
Reaction free energy (ΔG/kJ·mol^{-1}), dissociation free barrier (ΔG_a/kJ·mol^{-1}), desorption free energy (G_{des}/kJ·mol^{-1}), and the rate constants of dissociation and desorption (k_{dis} and k_{des}) at 500 and 550 K for CO dissociation at different coverage over Cu(100) surface in vacuum phase and liquid paraffin.

	Dissociation route	500 K					550 K				
		ΔG	ΔG_a	G_{des}	k_{dis}	k_{des}	ΔG	ΔG_a	G_{des}	k_{dis}	k_{des}
Vacuum	1CO → 1C + 1O	195.4	328.2	125.6	5.28×10^{-22}	0.78	196.9	329.1	128.6	6.24×10^{-19}	7.03
	2CO → 1CO + 1C + 1O	204.5	343.9	124.0	1.23×10^{-23}	1.15	205.7	348.1	128.0	9.84×10^{-21}	7.43
	1CO + 1C + 1O → 2C + 2O	221.8	353.4	125.0	1.24×10^{-24}	0.90	224.7	355.5	129.3	1.98×10^{-21}	6.01
	3CO → 2CO + 1C + 1O	217.2	335.6	122.9	8.93×10^{-23}	1.64	219.7	338.8	126.9	7.52×10^{-20}	9.17
	2CO + 1C + 1O → 1CO + 2C + 2O	241.0	355.5	110.2	7.43×10^{-25}	33.57	242.9	355.5	112.9	1.95×10^{-21}	2.20×10^{2}
	1CO + 2C + 2O → 3C + 3O	185.6	322.1	90.9	2.33×10^{-21}	3.50×10^{3}	183.8	317.9	94.6	7.28×10^{-18}	1.20×10^{4}
Liquid paraffin	1CO → 1C + 1O	175.1	318.5	182.8	5.43×10^{-21}	8.29×10^{-7}	174.0	317.7	190.0	7.65×10^{-18}	1.03×10^{-5}
	2CO → 1CO + 1C + 1O	189.9	344.8	119.2	9.91×10^{-24}	3.66	182.1	346.2	121.7	1.50×10^{-20}	31.40
	1CO + 1C + 1O → 2C + 2O	213.5	325.2	104.9	1.09×10^{-21}	1.15×10^{2}	216.4	327.3	114.2	9.43×10^{-19}	1.64×10^{2}
	3CO → 2CO + 1C + 1O	183.1	328.9	97.9	4.46×10^{-22}	6.16×10^{2}	181.9	329.3	102.2	6.04×10^{-19}	2.26×10^{3}
	2CO + 1C + 1O → 1CO + 2C + 2O	198.2	376.6	96.2	4.68×10^{-27}	9.24×10^{2}	200.3	382.9	93.8	4.89×10^{-24}	1.40×10^{4}
	1CO + 2C + 2O → 3C + 3O	226.5	330.5	56.8	3.08×10^{-22}	1.22×10^{7}	226.7	332.2	58.9	3.24×10^{-19}	2.89×10^{7}

Above results show that only H_2 adsorption with the parallel mode at the 4-fold hollow site is the dissociative adsorption, whereas, in other five adsorption structures, H_2 molecules are far away from the surface, which accords with the experiments that H_2 molecule is weak adsorption behavior [70]. Namely, only the parallel H_2 adsorption at the 4-fold hollow site can dissociate into two H atoms, which agrees with previous studies that the most favorable molecular orientation for H_2 dissociation is to keep the H-H axis parallel to Cu(100) surface [71].

For H atom, as shown in Fig. S3(c), the adsorption energies at the top, bridge, 4-fold hollow sites are 196.7, 239.5 and 244.1 kJ·mol^{-1}, respectively, similar to the previous results (183.3, 226.7 and 235.4 kJ·mol^{-1}) [62]. Thus, H atom prefers to adsorb at the 4-fold hollow site, however, the adsorption energies between the bridge site and 4-fold hollow site differs by only 4.8 kJ·mol^{-1}, which agree with previous findings that H atom is expected to be mobile on Cu surface [62,72].

3.1.5. Adsorptions of H_2 at different coverage

Similar to CO, all H_2 molecule with the parallel mode at the 4-fold hollow site in their initial configurations have been examined, the adsorption possibilities at different coverage are presented in Fig. S4. The most stable adsorption configurations of H_2 at different coverage and the stepwise adsorption energies are presented in Fig. 4.

For $n_{H2} = 2$ and 3, both are the dissociative adsorption after geometry optimization, and the dissociated H atoms are located at the bridge and 4-fold hollow sites, namely, the lateral repulsive interaction

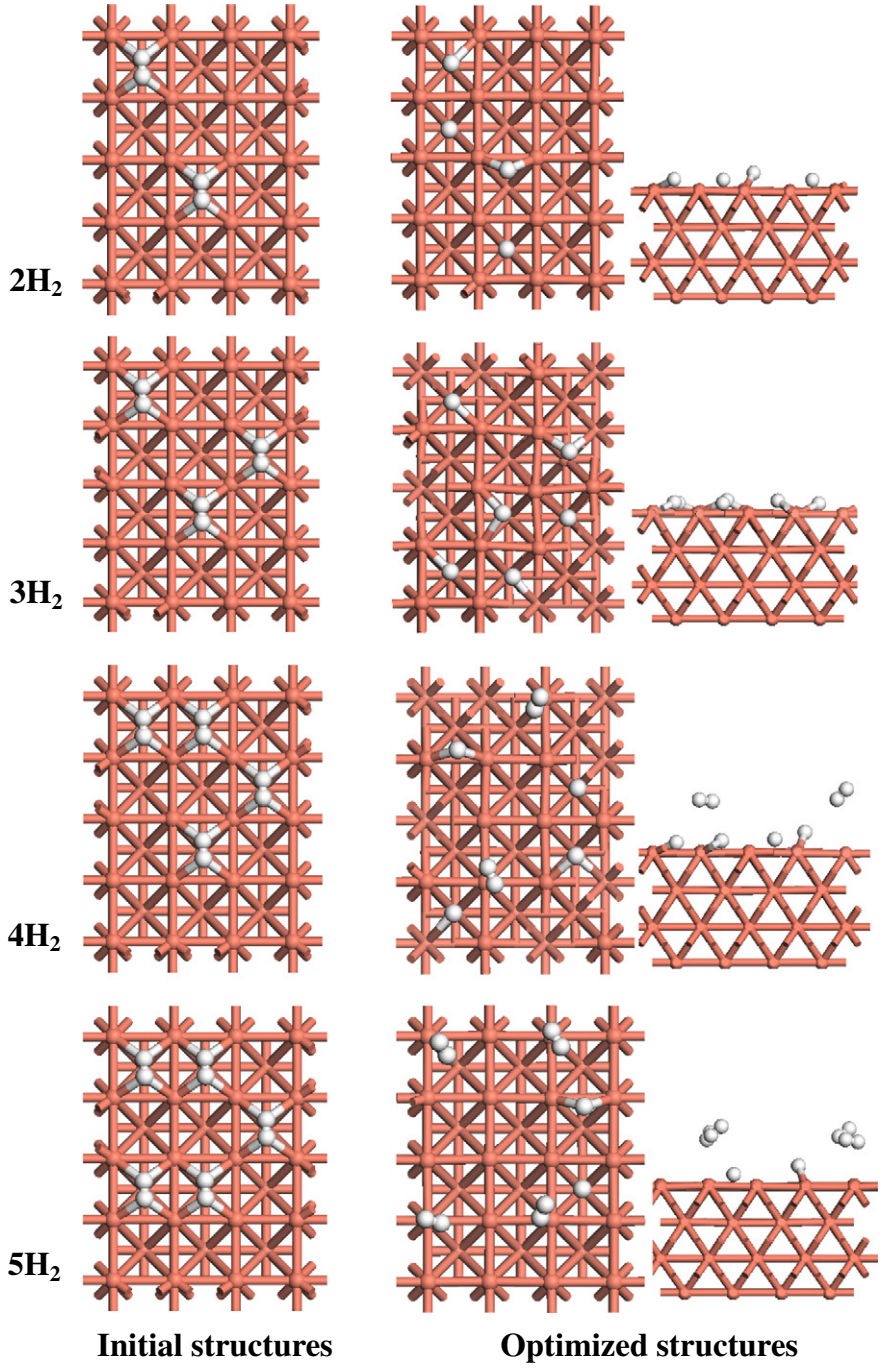

Fig. 4. The initial and optimized adsorption configurations for the most stable adsorbed H_2 molecules with the parallel mode at the 4-fold hollow site at the coverage from 2/12 to 5/12 ML over Cu(100) surface in vacuum.

between the dissociated H atoms gradually affects its adsorption site. Thus, H_2 is the dissociative adsorption at the coverage less than or equal to 3/12 ML over Cu(100) surface.

When four H_2 molecules are adsorbed on the surface, two H_2 molecules and four H atoms are adsorbed on Cu(100) surface because of the repulsive interaction. Further, molecular H_2 still exists at the coverage of 5/12 ML, in which four H_2 molecules and two H atoms are adsorbed on Cu(100) surface. Therefore, the saturated dissociative adsorption of H_2 over Cu(100) surface corresponds to the coverage of 3/12 ML. In addition, previous findings also showed that H_2 undergoes the dissociative adsorption on Cu(111) surface [73]. Zuo et al. [29] have studied the adsorption of the single H_2 on different $p(2 \times 2)$ Cu surfaces, while these models fail to describe the low coverage and thus ignore the dissociative adsorption of H_2 at low coverage in vacuum.

3.2. CO and H_2 adsorption under liquid paraffin condition

3.2.1. Adsorption of the single CO, C, and O

The most stable adsorption configurations of CO, C and O on Cu(100) surface are calculated in liquid paraffin using COSMO models. As shown in Fig. S5, CO prefers to adsorb at the bridge site via C atom with the adsorption energy of 150.0 kJ·mol^{-1}, which is slightly larger than that at the top site (142.8 kJ·mol^{-1}) and the 4-fold hollow site (148.4 kJ·mol^{-1}). Moreover, the C—O bonds at the top, bridge, 4-fold hollow sites are oriented perpendicularly to the surface with its length elongated to 1.168, 1.188 and 1.211 Å from 1.141 Å in gas phase, respectively, which agree well with the previous studies [27].

Both C and O atoms are preferentially adsorbed at the 4-fold hollow sites, as shown in Fig. S5 (b) and S5 (c). The corresponding adsorption energies of C and O atoms are 629.1 and 540.2 kJ·mol^{-1}, respectively; the average lengths of C—Cu and O—Cu bonds are 1.932 and 2.051 Å, respectively. The initial configurations of C and O atoms placed at the bridge and top sites are converted into that at the 4-fold hollow adsorptions after geometry optimization.

3.2.2. Adsorptions of CO at different coverage

For CO adsorption at different coverage in liquid paraffin, similar to that in vacuum, all CO adsorption possibilities located at the bridge and top site in their initial configurations with a given coverage have been examined, as presented in Figs. S6 and S7. The most stable adsorption configurations and the stepwise adsorption energies (ΔE_{ads}) are presented in Fig. 5.

For $n_{CO} = 1$ and 2, the stepwise adsorption energies (150.0 and 115.4 kJ·mol^{-1}) decrease sharply, while CO are still adsorbed at the bridge site with the C—O bond vertical to the surface. For $n_{CO} = 3$–4, CO molecules are also adsorbed at the bridge site, however, the stepwise adsorption energies (82.6 and 78.1 kJ·mol^{-1}) are obviously smaller than those of the first two CO.

For $n_{CO} = 5$ and 6, the stepwise adsorption energies ΔE_{ads} (69.9 and 69.5 kJ·mol^{-1}) gradually decreases, but all CO migrate from the bridge to the top site. For $n_{CO} = 7$, all CO are located at the top site with the stepwise adsorption energy of 66.4 kJ·mol^{-1}. For $n_{CO} = 8$, three CO molecules are adsorbed at the bridge site, and five CO molecules are adsorbed at the top site; the corresponding stepwise adsorption energy is 71.4 kJ·mol^{-1}. For $n_{CO} = 9$, ΔE_{ads} (−18.6 kJ·mol^{-1}) becomes negative, indicating that CO reaches the saturated adsorption at 8/12 ML.

Above results show that with the increasing of CO coverage, the stepwise adsorption energies of CO decreases, namely, CO desorption becomes easier over Cu(100) surface. Moreover, CO migrate from the bridge to top site.

3.2.3. Dissociation and desorption of CO at different coverage

Similar to CO dissociation in vacuum, we calculate the dissociation and desorption of CO at different coverage in liquid paraffin, as shown in Fig. 6. For the adsorption of CO at different coverage over Cu(100) surface in liquid paraffin, the dissociation barrier, reaction energy and desorption energy obtained from DFT calculations are listed in Table 1, and the dissociation free energy, reaction free barrier and desorption free energy, as well as the desorption and dissociation rate constants at 500 and 550 K are listed in Table 2. In addition, the potential energy profiles for the dissociation of CO, 2CO and 3CO molecules on Cu(100) surface in liquid paraffin have been presented in Fig. S10.

For one CO molecule dissociation on the surface, the adsorbed CO dissociates via transition state TS2-1 into C and O atoms; this elementary reaction is highly endothermic by 180.9 kJ·mol^{-1}, and the dissociation barrier is higher than its desorption energy (328.2 vs. 150.0 kJ·mol^{-1}), indicating that CO dissociation at 1/12 ML is obviously unfavorable both kinetically and thermodynamically than its desorption.

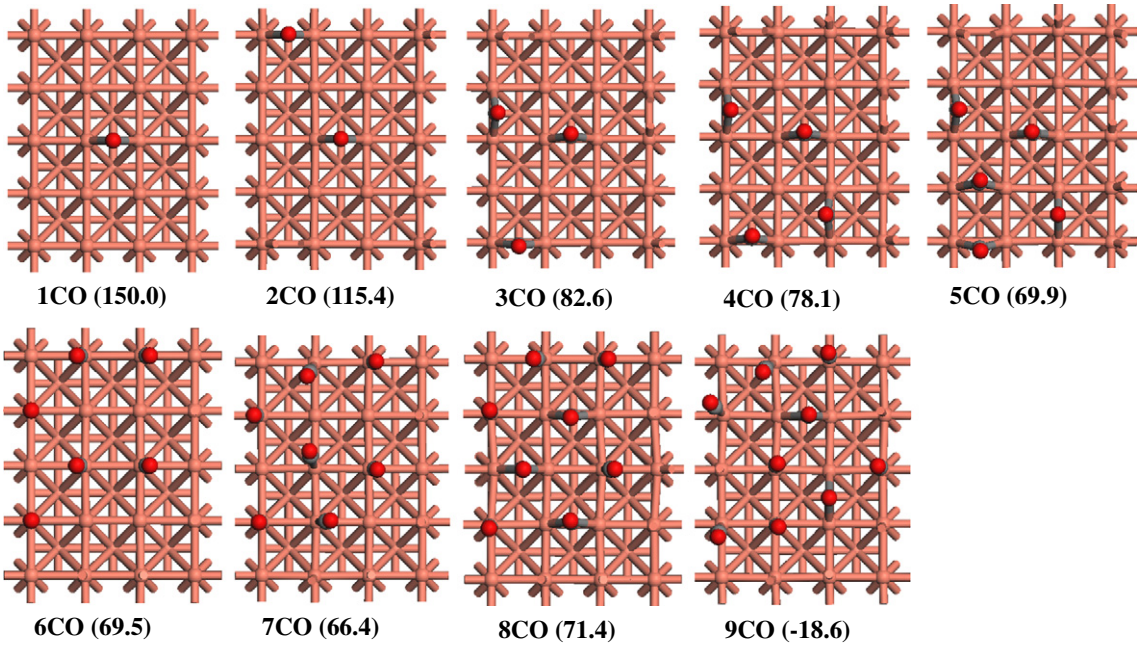

Fig. 5. The most stable adsorption configurations and energies of the stepwise CO adsorption on Cu(100) surface in liquid paraffin (unit: kJ·mol^{-1}).

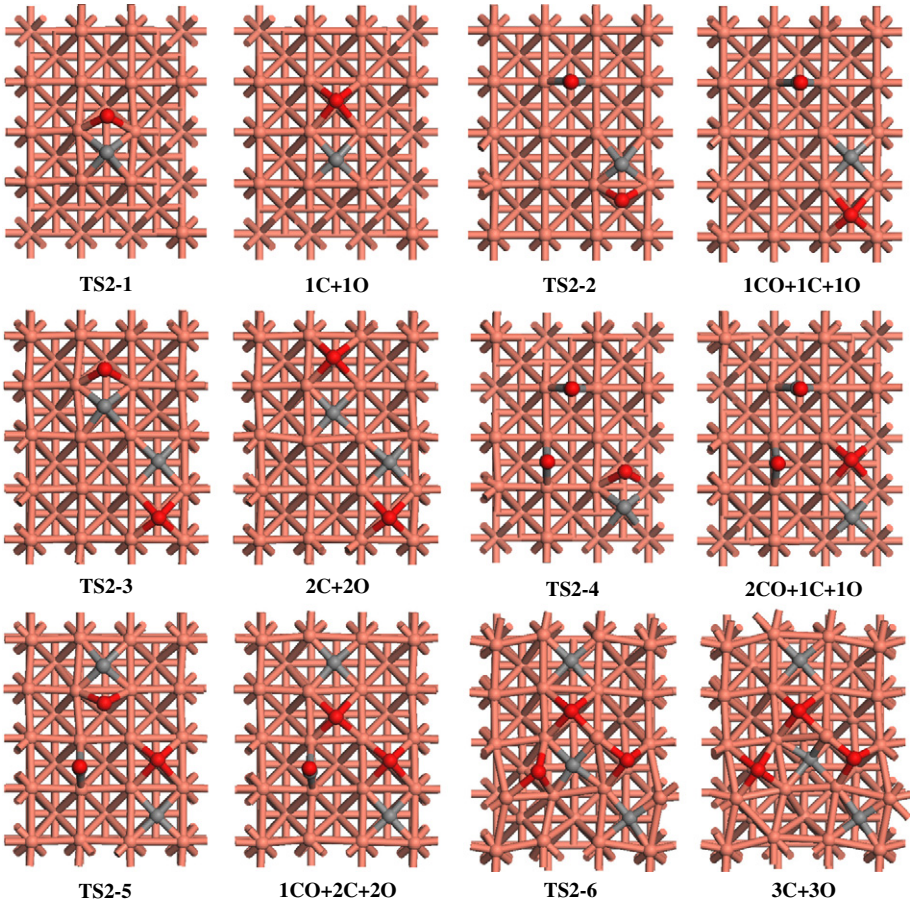

Fig. 6. Structures involved in the dissociations of 1–3 CO molecules on Cu(100) surface in liquid paraffin.

For two CO molecules dissociation, the adsorbed CO dissociates into 2C + 2O via transition states TS2–2 and TS2–3, respectively. The dissociation barriers of these two CO molecules (344.7 and 318.4 kJ·mol^{-1}) are much higher than the corresponding desorption energies (115.4 and 98.8 kJ·mol^{-1}), and the dissociation of these two CO molecules are endothermic by 198.0 and 192.4 kJ·mol^{-1}, respectively. Our results show that CO dissociation is also obviously unfavorable than its desorption at 2/12 ML.

For $n_{CO} = 3$, these CO molecules stepwise dissociate successively into three C and three O atoms via the transition states TS2-4 ~2–6 with the reaction energies of 199.5, 189.1 and 224.3 kJ·mol^{-1}, respectively; the dissociation barriers (349.6, 340.6 and 323.7 kJ·mol^{-1}) are higher than the stepwise desorption energies (82.6, 72.6 and 48.9 kJ·mol^{-1}), suggesting that CO dissociation is still difficult at the coverage of 3/12 ML.

On the basis of above results, it can be found that the dissociation barriers of CO at the coverage from 1/12 to 3/12 ML are much larger than the desorption barriers in liquid paraffin, and at a given coverage, the desorption barriers decrease with the increasing of C and O coverage. Similarly, the dissociation free barrier and desorption free energy, as well as the corresponding rate constants at different coverage also indicate the dissociation of CO is more difficult than its desorption at different temperature of 500 and 550 K. Meanwhile, the dissociation rate constants of the second CO dissociation decrease with the increasing of the coverage; moreover, with the increasing of the temperature, the desorption and dissociation rate constant increases, while the changes of the desorption rate constant become small. Thus, we can predict that CO dissociation will become difficult compared to its desorption when the coverage is greater than 3/12 ML.

3.2.4. Adsorption of the single H_2 and H species

As shown in Fig. S8, three parallel and three vertical modes are adsorbed at the top, bridge and 4-fold hollow in liquid paraffin, respectively. For the parallel mode, as shown in Fig. S8(a), H_2 adsorption at the top and bridge sites are converted to the corresponding vertical modes after geometry optimization, while the parallel adsorption at the 4-fold hollow site is the dissociative adsorption with two H atoms adsorbed at bridge site. However, for the vertical mode, as shown in Fig. S8(b), the adsorption configurations at the top, bridge and 4-fold hollow are still vertical with the adsorption energies of 53.9, 55.3 and 53.0 kJ·mol^{-1}, respectively. Meanwhile, the H—H bond lengths are elongated to 0.752, 0.755 and 0.753 Å compared to 0.747 Å in gas phase.

Above results show that only the parallel mode of H_2 adsorption at the 4-fold hollow site over Cu(100) surface in liquid paraffin is the dissociative adsorption into two H atoms, while H_2 in other five structures dominantly focus on the vertical mode with the adsorption energy about 53.0 kJ·mol^{-1}. Correspondingly, the dissociative adsorption structures of H_2 at different coverage are discussed in liquid paraffin to compare with the results in vacuum.

For H atom adsorption, the adsorption energies are 419.6, 431.3 and 439.5 kJ·mol^{-1} at the top, 4-fold hollow and bridge sites, respectively, as shown in Fig. S8(c), indicating that H atom prefers to mobilize on Cu surface in liquid paraffin due to the close adsorption energies.

3.2.5. Adsorption H_2 at different coverage

The adsorption possibilities of H_2 at different coverage are presented in Fig. S9. The most stable adsorption configurations of H_2 at different coverage and the stepwise adsorption energies are presented in Fig. 7.

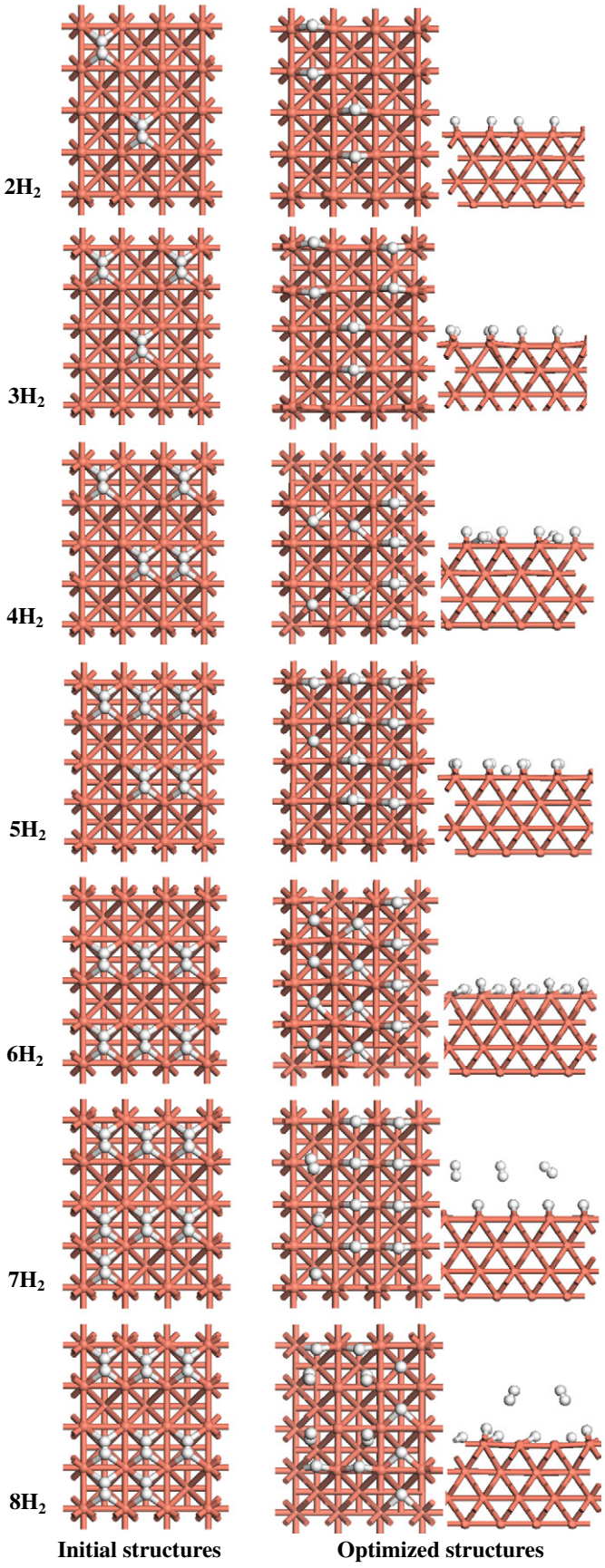

Fig. 7. The initial and optimized adsorption configurations for the most stable adsorbed H_2 molecules with the parallel mode at the 4-fold hollow site at the coverage from 2/12 to 8/12 ML over Cu(100) surface in liquid paraffin, respectively.

For the first three adsorbed H_2, all H_2 molecules are the dissociative adsorption with H atoms adsorbed at the bridge site, suggesting that the lateral repulsive interactions between the dissociated H atoms are negligible at the coverage less than or equal to 3/12 ML in liquid paraffin.

For $n_{H2} = 4$–6, as shown in Fig. 7, all H_2 molecules are still the dissociative adsorption, the dissociated H atoms are not only located at the bridge sites, but also adsorbed at the 4-fold hollow sites, suggesting that the lateral repulsive interaction affects the adsorption sites of H atoms over the surface.

When 7 H_2 molecules are adsorbed, H_2 molecular adsorption begins to appear on the surface due to the stronger repulsive interaction, where two H_2 molecules and ten H atoms are adsorbed at the bridge site; H_2 molecular adsorption still exists for 8 H_2 molecules. Thus, the saturated dissociative adsorption of H_2 over Cu(100) surface corresponds to the coverage of 6/12 ML.

3.3. General discussion

3.3.1. The effect of coverage and solvent on CO adsorption

On the basis of above results, Fig. 8 reflects the effect of CO coverage on the stepwise adsorption energy at different coverage in vacuum and liquid paraffin, where the saturated coverage of CO adsorption is 8/12 ML.

The single CO molecule prefers to adsorb at the bridge site in both vacuum and liquid paraffin conditions. Under two different conditions, the Cu—C and C—O bond lengths of the most favorable CO adsorption configuration are similar, however, there is significant difference of the adsorption energies. The adsorption energy of the single CO molecule in liquid paraffin (150.0 $kJ \cdot mol^{-1}$) is much larger than that in vacuum (102.4 $kJ \cdot mol^{-1}$), indicating that the stability of CO adsorption can be improved by solvent effect, which agrees with the previous results [19].

For two adsorbed CO molecules, the stepwise adsorption energy of the second CO molecule (101.7 $kJ \cdot mol^{-1}$) is nearly equal to the first CO molecule (102.4 $kJ \cdot mol^{-1}$) in vacuum; however, in liquid paraffin, there is great gap between the second CO molecule (115.4 $kJ \cdot mol^{-1}$) and the first CO molecule (150.0 $kJ \cdot mol^{-1}$). Thus, although CO stability rapidly reduces in liquid paraffin at the low coverage of 2/12 ML, CO stability in liquid paraffin is still stronger than that in vacuum.

When the coverage is greater than or equal to 3/12 ML, the adsorption energy in liquid paraffin is smaller than that in vacuum, suggesting that compared to the vacuum conditions, solvent effect cannot continue to facilitate CO adsorption. Namely, solvent effect only can improve the stability of CO adsorption at lower coverage.

As shown in Fig. 8, with the increasing of CO coverage, the stepwise adsorption energies decrease in vacuum and liquid paraffin due to the strong CO lateral repulsive interactions. In vacuum, the stepwise adsorption energies of CO decrease slowly at the coverage of less than or equal to 4/12 ML, however, it began to obviously decrease at the coverage from 5/12 to the saturated adsorption 8/12 ML. Comparatively, in liquid paraffin, the stepwise adsorption energies of CO rapidly decrease at the coverage of less than 4/12 ML, however, it slowly decrease at the coverage from 5/12 to the saturated adsorption 8/12 ML.

Further, improving the stability of CO adsorption means the increasing of the desorption energies, which may lead to CO dissociation more favorable than its desorption, namely, CO dissociation become easier. Our result shows that the higher dissociation barriers of CO at different coverage make CO dissociation difficult and unfavorable compared its desorption both in vacuum and liquid paraffin on Cu(100) surface; moreover, the desorption energies of CO molecules gradually decrease with the increasing of CO coverage. Thus, by comparisons between the dissociation and desorption, we can identify no matter what coverage you choose CO adsorption on Cu(100) surface, CO dissociation is always difficult and less favorable than its desorption under the vacuum and liquid paraffin conditions.

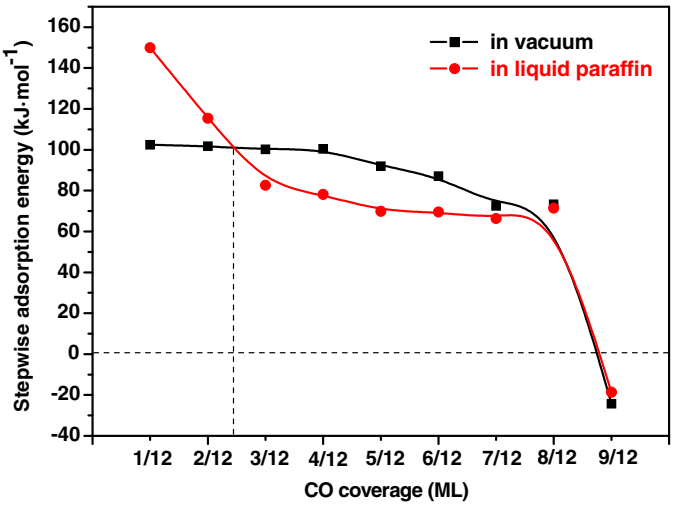

Fig. 8. The effect of CO coverage on its stepwise adsorption energy in vacuum and liquid paraffin.

Finally, based on the energies of CO adsorption at different coverage from DFT calculations, the effects of temperature and CO partial pressure have been considered, in which the adsorption Gibbs free energy was chosen as the criteria. Fig. 9 illustrates the relationship between the stable CO adsorption with the temperatures and CO partial pressure on Cu(100) surface at the equilibrium under the vacuum and liquid paraffin conditions, which clearly revealed that only molecular CO desorption is possible with the increasing of temperature at given pressure. In vacuum, there are three molecular adsorption regions and one CO free region; however, four molecular adsorption regions exist in liquid paraffin. Under the ultrahigh vacuum (UHV) conditions (10^{-14} to 10^{-9} atm; $\ln(p_{CO}/p^0) = -30.0 - -20.0$), the molecular adsorption CO starts to desorb in a narrow temperature range of 700–800 K in vacuum; however, in liquid paraffin, the molecular adsorption CO starts to desorb in a broad temperature range of 680–1130 K. By a comparison between Fig. 9(a) and (b), it can be found that CO molecules can still adsorb on Cu(100) surface when the temperature surpass 800 K, suggesting that the stability of CO adsorption on Cu(100) surface can be significantly improved by solvent effect; moreover, owing to solvent effect, the desorption of CO molecules in liquid paraffin is slower than that in vacuum with the increasing of temperature. At high pressure (1 atm), CO molecules can't be desorbed from Cu(100) surface at any given temperature range from 0 to 2000 K under the vacuum and liquid paraffin conditions, respectively.

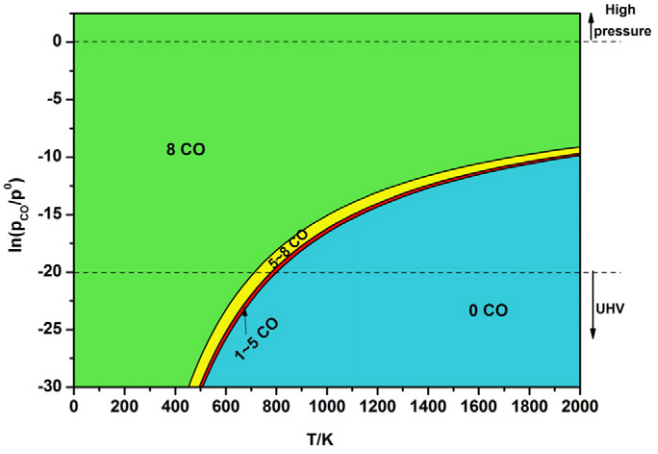

Fig. 9. Equilibrium phase diagram of the stable CO coverage with the temperatures and CO partial pressures on Cu(100) surface in (a) vacuum and (b) liquid paraffin.

3.3.2. The effect of coverage and solvent on H_2 adsorption

For a single H_2 molecule, in liquid paraffin, H_2 adsorption with the parallel mode at the top and bridge sites are converted to the corresponding vertical modes after geometry optimization, whereas it didn't occur in vacuum. However, in vacuum and liquid paraffin conditions, H_2 adsorption with the parallel mode at the 4-fold hollow site is the dissociative adsorption.

For more H_2 molecules at different coverage, all adsorbed H_2 is the dissociative adsorption at the coverage less than or equal to 3/12 ML in vacuum, whereas they are still the dissociative adsorption until to 6/12 ML in liquid paraffin, indicating that solvent effect make more H_2 molecules become the dissociative adsorption into H atoms.

With the increasing of H_2 coverage, the dissociated H atom will hinder the dissociative adsorption of H_2 due to the lateral repulsive interaction, thus, molecular adsorption H_2 begins to appear at high coverage. Compared to vacuum condition, solvent effect weakens the lateral repulsive interactions between the dissociated H atoms, more H_2 molecules in liquid paraffin become the dissociative adsorption. Moreover, all dissociated H atoms in liquid paraffin have few surface migrations than that in vacuum, suggesting that solvent effect is also in favor of stabilizing the adsorption configurations.

Fig. 10 illustrates the relationship between the stable H adsorption with the temperatures and H_2 partial pressure on Cu(100) surface at the equilibrium under the vacuum and liquid paraffin conditions, suggesting that the stable H coverage decreases upon the increasing of temperature at given pressures. On the basis of the equilibrium phase

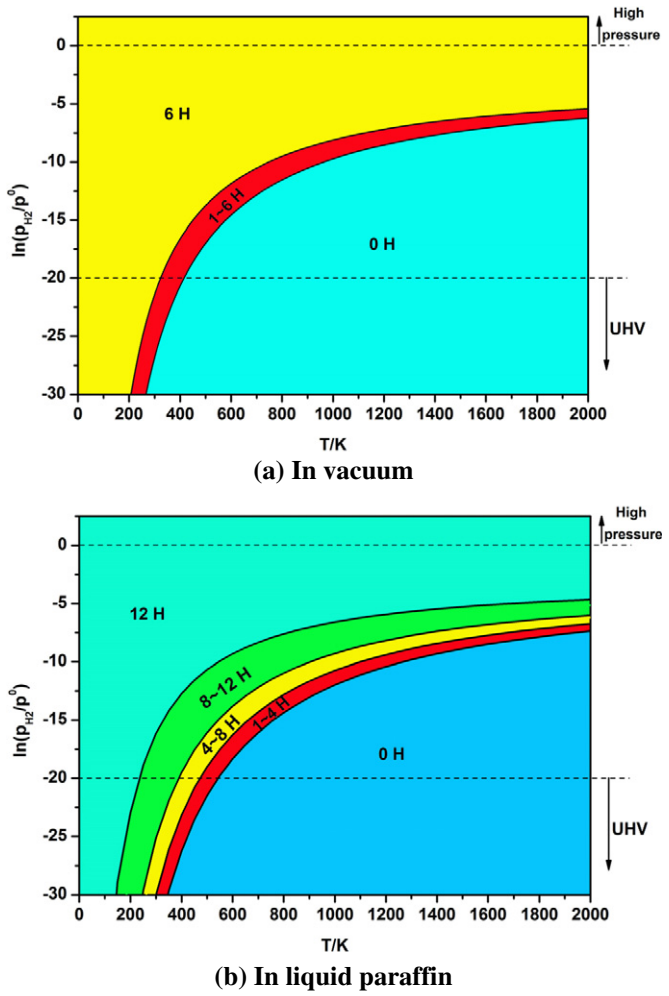

Fig. 10. Equilibrium phase diagram of the stable H coverage with the temperatures and H_2 partial pressures on Cu(100) surface in (a) vacuum and (b) liquid paraffin.

diagram of H coverage, one can directly get the stable H coverage under any given T andp_{H_2}. Similarly, we also compared the difference between Fig. 10(a) and (b), indicating that under the ultrahigh vacuum (UHV) conditions, the adsorbed H starts to desorb in a narrow temperature range of 300–400 K in vacuum, namely, H_2 molecules can spontaneously dissociate into H atoms in a narrow temperature range of 300–400 K in vacuum. However, in liquid paraffin, more dissociative adsorption regions exist, and H_2 molecules start to dissociate into H atoms in a broad temperature range of 200–500 K. Moreover, owing to solvent effect, the desorption of H atoms in liquid paraffin is slower than that in vacuum with the increasing of temperature.

In summary, our results show that for CO adsorption on Cu(100) surface, no matter under what coverage and reaction conditions, CO dissociation is always difficult and less favorable both kinetically and thermodynamically than its desorption. Whereas H_2 is the dissociative adsorption into H atoms, namely, H_2 exist in the form of H atoms on Cu catalyst under the realistic condition. Therefore, molecular adsorption CO and dissociative adsorption H_2 into H atoms exist on Cu catalyst in vacuum or liquid paraffin. These results can illustrate the essential roles of dissociative adsorption and molecular adsorption played in the process of H_2 and CO activation, respectively, and provide reasonable explanations for many studies related to CO and H_2 on Cu surface, in which H_2 is based on the H atoms rather than H_2 molecule, and CO is based on the molecular adsorption [37,65]. In addition, this study can also provide the useful information for the studies about syngas ($CO + H_2$) conversion on other metal catalysts.

4. Conclusions

As a key initial step in many catalytic reactions, the effect of coverage on the adsorption and activation of CO and H_2 over a $p(3 \times 4)$ Cu(100) surface model using DFT method, and the effect of the temperature and CO/H_2 partial pressure on CO/H_2 coverage have been investigated in vacuum and liquid paraffin conditions within atomistic thermodynamics.

As CO coverage increase from the lowest coverage (1/12 ML) to the saturated coverage (8/12 ML), the stepwise adsorption energies gradually decrease in vacuum and liquid paraffin and the adsorption site of CO molecules changes from the bridge site to the top site. Solvent effect can improve the stability of adsorbed CO at low coverage. Further, CO desorption become more facile than dissociation under different environmental conditions. On the other hand, H_2 is the dissociative adsorption when the coverage is less than or equal to 3/12 ML in vacuum and 6/12 ML in liquid paraffin. Under different temperatures and CO/H_2 partial pressures, the relationship of the stable CO/H_2 adsorption with the temperatures and CO/H_2 partial pressure on Cu(100) surface has been identified in vacuum and liquid paraffin conditions, respectively.

Generally, molecular adsorption CO and the dissociative adsorption H_2 into H atoms exist on Cu catalyst under the realistic condition in vacuum or liquid paraffin, namely, H_2 exists in the form of dissociated H atoms, and CO dominantly presents molecular state. Finally, this study can also provide the useful information for the studies about syngas ($CO + H_2$) conversion on other metal catalysts.

Acknowledgment

This work is financially supported by the National Natural Science Foundation of China (No. 21276003, 21476155 and 21276171), the Natural Science Foundation of Shanxi Province (No. 2014011012-2), the Program for the Top Young Academic Leaders of Higher Learning Institutions of Shanxi, and the Top Young Innovative Talents of Shanxi.

Appendix A. Supplementary data

A detailed descriptions about the effect of surface strain and the functional on CO adsorption at different coverage, the test results of Cu(100) surface model, ab initio atomistic thermodynamics, thermodynamic and rate constant calculations, as well as all possible initial configurations, their corresponding optimized structures of adsorbed CO and H_2 molecules at different coverage, and the potential energy profiles of 1–3 CO dissociation over Cu(100) surface in vacuum and liquid paraffin have been presented. Supplementary data associated with this article can be found in the online version, at http://dx.doi.org/10.1016/j.fuproc.2016.09.005.

References

[1] J.J. Spivey, A. Egbebi, Heterogeneous catalytic synthesis of ethanol from biomass-derived syngas, Chem. Soc. Rev. 36 (2007) 1514–1528.
[2] K.G. Fang, D.B. Li, M.G. Lin, M.L. Xiang, W. Wei, Y.H. Sun, A short review of heterogeneous catalytic process for mixed alcohols synthesis via syngas, Catal. Today 147 (2009) 133–138.
[3] I. Wender, Reactions of synthesis gas, Fuel Process. Technol. 48 (1996) 189–297.
[4] Z.J. Zuo, W. Huang, P.D. Han, Z.H. Li, Solvent effects for CO and H_2 adsorption on $Cu_2O(111)$ surface: a density functional theory study, Appl. Surf. Sci. 256 (2010) 2357–2362.
[5] Z.H. Gao, W. Huang, L.H. Yin, K.C. Xie, Liquid-phase preparation of catalysts used in slurry reactors to synthesize dimethyl ether from syngas: effect of heat-treatment atmosphere, Fuel Process. Technol. 90 (2009) 1442–1446.
[6] C. Arcoumanis, C. Bae, R. Crookes, E. Kinoshita, The potential of di-methyl ether (DME) as an alternative fuel for compression-ignition engines: a review, Fuel 87 (2008) 1014–1030.
[7] A. Galadima, O. Muraza, From synthesis gas production to methanol synthesis and potential upgrade to gasoline range hydrocarbons: a review, J. Nat. Gas Sci. Eng. 25 (2015) 303–316.
[8] X.J. Guo, L.M. Li, S.M. Liu, G.L. Bao, W.H. Hou, Preparation of $CuO/ZnO/Al_2O_3$ catalysts for methanol synthesis using parallel-slurry-mixing method, J. Fuel Chem. Technol. 35 (2007) 329–333.

[9] M. Gupta, M.L. Smith, J.J. Spivey, Heterogeneous catalytic conversion of dry syngas to ethanol and higher alcohols on Cu-based catalysts, ACS Catal. 1 (2011) 641–656.
[10] H. Yue, X. Ma, J. Gong, An alternative synthetic approach for efficient catalytic conversion of syngas to ethanol, Acc. Chem. Res. 47 (2014) 1483–1492.
[11] K. Okabe, K. Murata, M. Nakanishi, T. Ogi, M. Nurunnabi, Y.Y. Liu, Fischer–Tropsch synthesis over Ru catalysts by using syngas derived from woody biomass, Catal. Lett. 128 (2009) 171–176.
[12] D.A. Simonetti, J. Rass-Hansen, E.L. Kunkes, R.R. Soares, J.A. Dumesic, Coupling of glycerol processing with Fischer–Tropsch synthesis for production of liquid fuels, Green Chem. 9 (2007) 1073–1083.
[13] G.C. Wang, L. Jiang, Z.S. Cai, Y.M. Pan, X.Z. Zhao, W. Huang, K.C. Xie, Y.W. Li, Y.H. Sun, B. Zhong, Surface structure sensitivity of the water-gas shift reaction on Cu(hkl) surfaces: a theoretical study, J. Phys. Chem. B 107 (2003) 557–562.
[14] J.L. Gong, H.R. Yue, Y.J. Zhao, S. Zhao, L. Zhao, J. Lv, S.P. Wang, X.B. Ma, Synthesis of ethanol via syngas on Cu/SiO_2 catalysts with balanced Cu^0–Cu^+ sites, J. Am. Chem. Soc. 134 (2012) 13922–13925.
[15] J. Sun, S.L. Wan, F. Wang, J.D. Lin, Y. Wang, Selective synthesis of methanol and higher alcohols over $Cs/Cu/ZnO/Al_2O_3$ catalysts, Ind. Eng. Chem. Res. 54 (2015) 7841–7851.
[16] K. Krekkeitsakul, T. Utistham, U.W. Hartley, Methanol synthesis in a slurry phase reactor over $Cu/ZnO/Al_2O_3$ catalyst, Adv. Mater. Res. 931–932 (2014) 27–31.
[17] R.T. Figueiredo, A. Martınez-Arias, M.L. Granados, J. Fierro, Spectroscopic evidence of Cu–Al interactions in Cu–Zn–Al mixed oxide catalysts used in CO hydrogenation, J. Catal. 178 (1998) 146–152.
[18] J. Erena, R. Garoña, J.M. Arandes, A.T. Aguayo, J. Bilbao, Effect of operating conditions on the synthesis of dimethyl ether over a $CuO-ZnO-Al_2O_3$/NaHZSM-5 bifunctional catalyst, Catal. Today 107-108 (2005) 467–473.
[19] Z.J. Zuo, W. Huang, P.D. Han, Z.H. Li, Adsorption of CO on Cu(110) and (100) surfaces using COSMO-based DFT, J. Mol. Model. 15 (2009) 1079–1083.
[20] Z.H. Gao, W. Huang, L.F. Hao, K.C. Xie, Liquid-phase preparation of CuO/ZrO_2 catalyst used in slurry reactors and its catalytic activity for CO hydrogenation, Chin. J. Catal. 27 (2006) 86–90.
[21] S.R. Yu, Y.E. Chen, S.S. Gao, X.D. Wang, W. Huang, Ethanol synthesis from synthesis gas over complexing agent modified $Cu-ZnO/Al_2O_3$ prepared by complete liquid-phase technology, Energy Sources Part A 35 (2013) 955–961.
[22] G.C. Wang, L. Jiang, X.Y. Pang, Z.S. Cai, Y.M. Pan, X.Z. Zhao, Y. Morikawa, J.J. Nakamura, A theoretical study of surface-structural sensitivity of the reverse water-gas shift reaction over Cu(hkl) surfaces, Surf. Sci. 543 (2003) 118–130.
[23] M. Neef, K. Doll, CO adsorption on the Cu(111) surface: a density functional study, Surf. Sci. 600 (2006) 1085–1092.
[24] Z.J. Zuo, W. Huang, P.D. Han, Z.H. Li, CO and H_2 molecules adsorption on Cu(111) surface and solvent effects, Acta Phys. -Chim. Sin. 25 (2009) 2507–2512.
[25] Q. Fu, Y. Luo, Active sites of Pd-doped flat and stepped Cu(111) surfaces for H_2 dissociation in heterogeneous catalytic hydrogenation, ACS Catal. 3 (2013) 1245–1252.
[26] F. Göltl, C. Houriez, M. Guitou, G. Chambaud, P. Sautet, Importance of a nonlocal description of electron–electron interactions in modeling the dissociative adsorption of H_2 on Cu(100), J. Phys. Chem. C 118 (2014) 5374–5382.
[27] Z.J. Zuo, L. Sun, W. Huang, P.D. Han, Z.H. Li, Surface properties of copper in different solvent mother solutions: a density functional theory study, Appl. Catal. A Gen. 375 (2010) 181–187.
[28] J. Kessler, F. Thieme, Chemisorption of CO on differently prepared Cu(111) surfaces, Surf. Sci. 67 (1977) 405–415.
[29] Z.J. Zuo, W. Huang, P.D. Han, A DFT study the solvent effects of H_2 adsorption on Cu(hkl) surface, Appl. Surf. Sci. 258 (2012) 3364–3367.
[30] J. Cook, E. McCash, Vibrational energy-transfer processes in the COCu(100) system, Surf. Sci. 371 (1997) 213–222.
[31] T. Wang, X.X. Tian, Y.W. Li, J.G. Wang, M. Beller, H.J. Jiao, High coverage CO activation mechanisms on Fe(100) from computations, J. Phys. Chem. C 118 (2014) 1095–1101.
[32] T. Wang, S.G. Wang, Y.W. Li, J.G. Wang, H.J. Jiao, Adsorption equilibria of CO coverage on β-Mo_2C surfaces, J. Phys. Chem. C 116 (2012) 6340–6348.
[33] T. Wang, S.G. Wang, Q.Q. Luo, Y.W. Li, J.G. Wang, M. Beller, H.J. Jiao, Hydrogen adsorption structures and energetics on iron surfaces at high coverage, J. Phys. Chem. C 118 (2014) 4181–4188.
[34] P. Zhao, Y.R. He, D.B. Cao, X.D. Wen, H.W. Xiang, Y.W. Li, J.G. Wang, H.J. Jiao, High coverage adsorption and co-adsorption of CO and H_2 on Ru(0001) from DFT and thermodynamics, Phys. Chem. Chem. Phys. 17 (2015) 19446–19456.
[35] T. Wang, X.X. Tian, Y.W. Li, J.G. Wang, M. Beller, H.J. Jiao, Coverage-dependent CO adsorption and dissociation mechanisms on iron surfaces from DFT computations, ACS Catal. 4 (2014) 1991–2005.
[36] T. Wang, X.X. Tian, Y. Yang, Y.W. Li, J.G. Wang, M. Beller, H.J. Jiao, Structures of seven molybdenum surfaces and their coverage dependent hydrogen adsorption, Phys. Chem. Chem. Phys. 18 (2016) 6005–6012.
[37] L. Grabow, M. Mavrikakis, Mechanism of methanol synthesis on Cu through CO_2 and CO hydrogenation, ACS Catal. 1 (2011) 365–384.
[38] P.L. Hansen, J.B. Wagner, S. Helveg, J.R. Rostrup-Nielsen, B.S. Clausen, H. Topsøe, Atom-resolved imaging of dynamic shape changes in supported copper nanocrystals, Science 295 (2002) 2053–2055.
[39] B. Delley, An all-electron numerical method for solving the local density functional for polyatomic molecules, J. Chem. Phys. 92 (1990) 508–517.
[40] B. Delley, From molecules to solids with the $DMol^3$ approach, J. Chem. Phys. 113 (2000) 7756–7764.
[41] P. Liu, J.A. Rodriguez, Y. Takahashi, K. Nakamura, Water–gas-shift reaction on a $Ni_2P(001)$ catalyst: formation of oxy-phosphides and highly active reaction sites, J. Catal. 262 (2009) 294–303.
[42] J.P. Perdew, K. Burke, M. Ernzerhof, Generalized gradient approximation made simple, Phys. Rev. Lett. 77 (1996) 3865–3868.
[43] J.P. Perdew, Y. Wang, Accurate and simple analytic representation of the electron-gas correlation energy, Phys. Rev. B 45 (1992) 13244–13249.
[44] J. Pritchard, On the structure of CO adlayers on Cu(100) and Cu(111), Surf. Sci. 79 (1979) 231–244.
[45] B. Hammer, L.B. Hansen, J.K. Nørskov, Improved adsorption energetics within density-functional theory using revised Perdew–Burke–Ernzerhof functionals, Phys. Rev. B 59 (1999) 7413–7421.
[46] J.P. Perdew, K. Burke, M. Ernzerhof, Perdew, Burke, and Ernzerhof reply, Phys. Rev. Lett. 80 (1998) 891.
[47] D.E. Jiang, E.A. Carter, Adsorption and dissociation of CO on Fe(110) from first principles, Surf. Sci. 570 (2004) 167–177.
[48] M. Dolg, U. Wedig, H. Stoll, H. Preuss, Energy-adjusted abinitio pseudopotentials for the first row transition elements, J. Chem. Phys. 86 (1987) 866–872.
[49] R. Aziz, Molecular physics: an international journal at the interface between chemistry and physics, Mol. Phys. 38 (1979) 177.
[50] P. Hohenberg, W. Kohn, Inhomogeneous electron gas, Phys. Rev. 136 (1964) B864–B871.
[51] X.B. Hao, B.J. Wang, Q. Wang, R.G. Zhang, D.B. Li, Insight into both coverage and surface structure dependent CO adsorption and activation on different Ni surfaces from DFT and atomistic thermodynamics, Phys. Chem. Chem. Phys. 18 (2016) 17606–17618.
[52] C.B. Chen, Q. Wang, R.G. Zhang, B. Hou, D.B. Li, L.T. Jia, B.J. Wang, High coverage CO adsorption and dissociation on the Co(0001) and Co(100) surfaces from DFT and thermodynamics, Appl. Catal. A Gen. 523 (2016) 209–220.
[53] R.G. Zhang, F. Liu, X.J. Zhao, B.J. Wang, L.X. Ling, First-principles study about the effect of coverage on H_2 adsorption and dissociation over a Rh(100) surface, J. Phys. Chem. C 119 (2015) 10355–10364.
[54] A.V. Gavrilenko, T.D. Matos, C.E. Bonner, S.S. Sun, C. Zhang, V. Gavrilenko, Optical absorption of poly (thienylene vinylene)-conjugated polymers: experiment and first principle theory, J. Phys. Chem. C 112 (2008) 7908–7912.
[55] T.A. Halgren, W.N. Lipscomb, The synchronous-transit method for determining reaction pathways and locating molecular transition states, Chem. Phys. Lett. 49 (1977) 225–232.
[56] K. Reuter, M. Scheffler, Composition, structure, and stability of $RuO_2(110)$ as a function of oxygen pressure, Phys. Rev. B 65 (2001), 035406-1-11.
[57] K. Reuter, M. Scheffler, Composition and structure of the $RuO_2(110)$ surface in an O_2 and CO environment: implications for the catalytic formation of CO_2, Phys. Rev. B 68 (2003), 045407-1-11.
[58] K.C. Waugh, Methanol synthesis, Catal. Today 15 (1992) 51–75.
[59] A.B. Stiles, F. Chen, J.B. Harrison, X.D. Hu, D.A. Storm, H.X. Yang, Catalytic conversion of synthesis gas to methanol and other oxygenated products, Ind. Eng. Chem. Res. 30 (1991) 811–821.
[60] J. Sun, S.L. Wan, F. Wang, J.D. Lin, Y. Wang, Selective synthesis of methanol and higher alcohols over $Cs/Cu/ZnO/Al_2O_3$ catalysts, Ind. Eng. Chem. Res. 54 (2015) 7841–7851.
[61] A. Hussain, Beneficial effect of Cu on a Cu-modified Au catalytic surface for CO oxidation reaction: a DFT study, J. Phys. Chem. C 117 (2013) 5084–5094.
[62] A.S.Y. Foo, K.H. Lim, Density functional study of the effects of strains on the adsorption of methoxide and its decomposed intermediates on Cu(100) surface, Catal. Lett. 127 (2009) 113–118.
[63] T. Wang, Y.W. Li, J.G. Wang, M. Beller, H.J. Jiao, High coverage CO adsorption and dissociation on the orthorhombic Mo_2C (100) surface, J. Phys. Chem. C 118 (2014) 3162–3171.
[64] L.J. Xu, D.H. Mei, G. Henkelman, Adaptive kinetic monte carlo simulation of methanol decomposition on Cu(100), J. Chem. Phys. 131 (2009), 244520-1-8.
[65] X.C. Sun, R.G. Zhang, B.J. Wang, Insights into the preference of CH_x($x = 1$–3) formation from CO hydrogenation on Cu(111) surface, Appl. Surf. Sci. 265 (2013) 720–730.
[66] A. Pavão, T. Guimaraes, S. Lie, C. Taft, W. Lester, Modeling the adsorption and dissociation of CO on transition metal surfaces, THEOCHEM J. Mol. Struct. 458 (1998) 99–121.
[67] E. Niemi, J. Nieminen, Channel selective scanning tunneling spectroscopy, Surf. Sci. 600 (2006) 2548–2554.
[68] H.L. Rouzo, P. Parneix, G. Raseev, K.S. Smirnov, Adsorption sites and migration of a carbon monoxide molecule on stepped vicinal surfaces of Cu(211) and Cu(511), Surf. Sci. 415 (1998) 131–147.
[69] H. Kao, M. Kawai, Switching in the molecular orientation ruled by steric repulsion of adsorbed CO on Pd(110), Phys. Rev. Lett. 82 (1999) 1899–1902.
[70] J. Pritchard, F. Tompkins, Surface potential measurements. The adsorption of hydrogen by group 1B metals, Trans. Faraday Soc. 56 (1960) 540–550.
[71] J.J. Xie, P. Jiang, K.M. Zhang, The dissociative adsorption of H_2 on Cu(100): orientation dependence and impurity effects, J. Phys. Condens. Matter 6 (1994) 7217–7226.
[72] Z.X. Chen, K.M. Neyman, K.H. Lim, N. Rösch, CH_3O decomposition on PdZn(111), Pd(111), and Cu(111). a theoretical study, Langmuir 20 (2004) 8068–8077.
[73] Y.X. Yang, J. Evans, J.A. Rodriguez, M.G. White, P. Liu, Fundamental studies of methanol synthesis from CO_2 hydrogenation on Cu(111), Cu clusters, and Cu/ZnO(0001), Phys. Chem. Chem. Phys. 12 (2010) 9909–9917.